Fractal analysis of seismoacoustic signals of near-surface sedimentary rocks in Kamchatka

Sanjar Imashev[1], Mikhail Mishchenko[2] and Mikhail Cheshev[1]

[1] Research Station of the Russian Academy of Sciences, Bishkek, Kyrgyzstan

[2] Institute of Cosmophysical Research and Radio Wave Propagation, Far East Branch of the Russian Academy of Sciences, Paratunka, Elizovskiy District, Kamchatka Region, Russia

We studied, by the mono- and multifractal detrended fluctuation analysis (DFA), time fluctuations in the dynamics of seismoacoustic data, recorded in Karymshina site, which is located in a seismic area of Kamchatka. We took a series of seismoacoustic responses to the regional seismic events with the magnitudes $M > 4$ for the period 2017–2018. The series was divided into three groups (high, medium and low) based on the amplitude of recorded seismoacoustic response. Background noise segments of the signals demonstrated monofractal behavior similar to white noise by almost constant values of generalized Hurst exponent $H_q \approx 0.5$ and very small width of the multifractal spectrum $\Delta\alpha \approx 0.1$. Analysis of the high amplitude seismoacoustic signals with clear P-, S- and coda waves showed that P- and S-waves demonstrate wider multifractal spectrum ($\Delta\alpha_P = 0.37$, $\Delta\alpha_S = 0.35$) and range of generalized Hurst exponents H_q in comparison with coda wave, characterized by almost constant H_q and minimal width of multifractal spectrum ($\Delta\alpha_{CODA} = 0.13$). We showed that the properties of the multifractal spectrum could be used in detection of seismic wave arrival, estimation its duration and separation of P-, S- and coda waves. Application of the monofractal DFA in a sliding window showed that the acoustic signal transits from monofractal and uncorrelated background noise (Hurst exponent equals to 0.5) into the long-range dependent state during seismic waves arrival, that is helpful in analysis of the signals, particularly in case of low amplitude acoustic responses, usually demonstrating an unclear waveform. Difference in multifractal spectrum width between the original low amplitude signal and its surrogates, obtained by random shuffling showed that the multifractality in the signal is dominantly due to long-range correlations.

Keywords: seismoacoustic signal, monofractal, Hurst exponent, multifractal, detrended fluctuation analysis

1. Introduction

In seismically active regions, where the continuous seismotectonic process is accompanied by more intensive deformations of rock, anomalous disturbances

of different geophysical fields are observed during earthquake preparation and might be considered as precursors (Adushkin and Spivak, 2012). Studies in Kamchatka (Larionov et al., 2014; Rulenko et al., 2014; Marapulets et al., 2011) showed that pre-seismic anomalous fluctuations in acoustic, atmospheric-electric and emanation fields occur as the result of relative microdisplacements of near-surface sedimentary rock fragments.

At present time, investigation of geophysical medium response on near-surface sedimentary rock deformation under different impact is topical. Seismic waves are used as the known impact on the geosphere. When they propagate, sedimentary rocks at an observation site suffer significant deformations. In this case, seismoacoustic effect, *i.e.* generation of acoustic signals as the result of relative mictrodisplacements of rock fragments and their interactions, should be observed. Seismoacoustic signal is supposed to contain several components: low-frequency seismic and high-frequency one, which reflect the sedimentary rock response during seismic wave passing through the measuring site. Based on the studies in this region (Kuptsov, 2005; Larionov et al., 2014), the sources of seismoacoustic signals are located at the distance of not more than tens of meters from the registration point and, evidently, are formed in the conditions of inhomogeneous plastic deformation which is accompanied by grain boundary sliding. This process is sensitive to dynamic disturbances, in particular, to seismic waves that makes it possible to use seismoacoustic signals as a sensitive indicator of seismic wave arrival (Dolgikh et al., 2007).

Several studies carried out to analyze acoustic emission signals using fractal approach, reporting that fractal dimension of acoustic emission series demonstrates decreasing up to catastrophic stage (Gregori et al., 2010; Carpinteri et al., 2009; Lu et al., 2005). Fractal analysis of acoustic emission registered near 'future' epicentral area, indicated evolution of the system before the main seismic event by progressive decrease of fractal dimension (Paparo et al., 2006). Carpinteri et al. (2009) performed fractal analysis of damage, detected in concrete structural elements by acoustic emission sensors, indicating decrease of fractal dimension and b-value as the damage develops.

In this study we investigate fractal properties of seismoacoustic signals, recorded during seismic wave passing through the measuring station on the basis of mono- and multifractal detrended fluctuation analysis (DFA), that give us an additional information about acoustic response to a seismic wave, especially for low amplitude signals, containing dominant noise component.

2. Instrumentation and data

Registration of seismoacoustic emission in Kamchatka are carried out at geophysical observation site Karymshina of IKIR FEB RAS (52.83° N, 158.13° E), located in the region of Verchne-Paratunskaya geothermal system of Southern

Kamchatka in the zone of intersection of different-rank tectonic faults. Based on the results of drilling and building works, the near-surface rocks at the observation site are sedimentary with the layer thickness of about 50 m and have fragmental structure (Kuptsov, 2005; Larionov et al., 2014).

The measurement system is arranged on the ground surface. The seismic receiver is mounted on the top of a casing pipe support of a dry five-meter well so that the oscillating acceleration vector components X and Y lie in the horizontal plane, Z is directed vertically upwards. The main part of the system is placed in a shelter at the distance of 10 m from the well.

To record the seismoacoustic emission signals, we apply a measuring system (Zakupin et al., 2014), which was developed and constructed at Research Station of the Russian Academy of Sciences. The system was upgraded to apply it on the ground surface and presented to IKIR FEB RAS within joint investigations. Figure 1 shows a scheme of seismoacoustic measurement system consisted of two joint parts: the remote and the main one. The remote part of the system consists of a signal sensor and cable amplifier block. It is arranged at the registration point and is connected to the main part by 20 m long special screened multi-cable. The main part includes an amplifier and filtration block, analog-to-digital conversion block and PC.

A three-component piezoceramic seismic receiver A-1638, manufactured by ZAO «Geoakustika», is used as a signal sensor (URL1). The sensor parameters are the following: conversion coefficient (≈ 1 V s^2 m^{-1}), maximal harmonic acceleration (≈ 5 m s^{-2}) and integral noise level in the pass band (10^{-5} m s^{-2}). The seismic receiver converts seismoacoustic signals into electric voltage proportional to oscillation acceleration in the frequency range from 0.2 to 400 Hz.

Signals from the sensor arrive at the inputs of cable amplifier block (CAB) which provides their undistorted and noise-free transmission though a long communication line to the input of the measurement complex. Then the signals are sent to the amplification and filtration block (AFB). Then, taking into the account the seismic receiver frequency characteristics, CAB and AFB blocks, signals in the frequency range of 0.5–400 Hz enter the inputs of the ADC block which is represented by analogue-to-digital converter L-CARD E14-140. Thus, the measurement system (Fig. 1) converts three orthogonal components (X, Y, Z) of oscillating acceleration vector into electric signal and records them with the sampling frequency of 1 kHz.
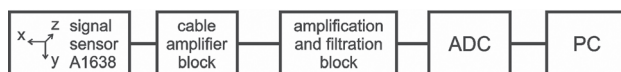
Figure 1. Scheme of the measurement system. ADC – analogue-to-digital conversion block, PC – personal computer.

Table 1. Seismic events.

Group	Event	Date and time	Coordinates (Lat., Long.)	Magnitude (M)
I	SE1	23.05.2018, 01:37:44:8	55.07, 162.44	5.7
	SE2	05.03.2018, 15:42:41:0	52.38, 160.80	5.1
II	SE3	29.12.2017, 19:20:45:0	50.03, 165.70	4.2
	SE4	15.10.2018, 16:45:05.6	48.91, 151.86	4.6
III	SE5	21.05.2018, 10:40:18:1	56.52, 161.46	4.7
	SE6	13.12.2017, 02:00:35:9	55.74, 161.48	4.4

We used the catalogue of regional earthquakes for 2017–2018 provided by Kamchatka Branch of the United Geophysical Survey of the Russian Academy of Sciences (http://www.emsd.ru) as the source of seismic event characteristics.
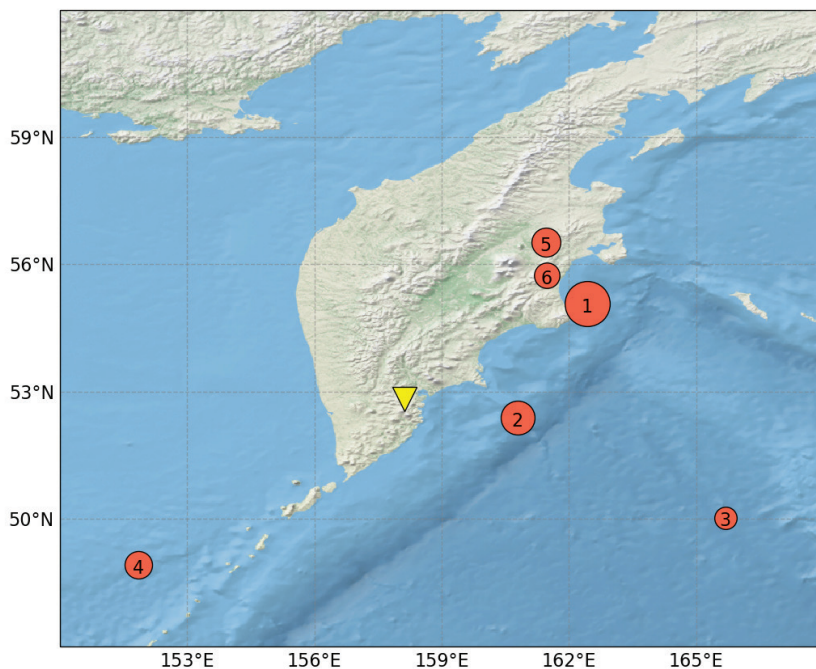
Figure 2. Location of the measuring station and selected events. Markers: triangle – Karymshina site; circles – epicenters (circle size corresponds to the earthquake magnitude).

We chose events with the magnitude $M > 4$ and separated them into three groups by relative amplitude of seismoacoustic response: high, medium and low amplitude events. For the sake of simplicity, we selected only two events per group for further analysis (Tab. 1). The first group includes high amplitude events SE1 and SE2, the second one – medium amplitude SE3 and SE4 and the third one – low amplitude signals SE5 and SE6.

Figure 2 shows the epicenters of the considered events in relation to Karymshina measuring site.

We analyzed the vertical component of seismoacoustic signals in each of the indicated groups, however, the horizontal components showed similar behavior.

3. Methodology

Acoustic response to seismic event contains waveform, trends and noise component that gives ground to apply methods of fractal analysis, which are used widely in analysis of signals, that could be potentially influenced by trends and nonstationarities, whose origin is often unknown (Gadre et al., 2014; Turcotte, 1997). In this case, the main advantage of fractal analysis is capability to investigate signals which, do not contain any useful information and are noisy, from the point of view of classical methods of covariance and spectral theories (Seuront, 2010). Registered seismoacoustic signals are characterized by complex waveform and surrounded by background noise. In case of low amplitude signals, the moment of seismic wave arrival is not clearly distinguished from the background noise. If the background noise is a stationary and uncorrelated series (Seuront, 2010; Padhy, 2016) and the waveform shows scale-dependent correlations in fluctuations, which are related to heterogeneities of the medium at different scales (Padhy, 2016) we can use mono- and multifractal characteristics to detect the moments of seismic wave arrival.

3.1. Monofractal detrended fluctuation analysis

We can analyze transition of acoustic signal from uncorrelated monofractal form to non-stationary correlated form by application of monofractal detrended fluctuation analysis (Peng et al., 1994; Kantelhardt et al., 2001).

The method was successfully applied in various studies of long-range power-law correlations, *e.g.* in DNA sequences (Buldyrev et al., 1995), temperature records (Talkner and Weber, 2000; Király and Jánosi, 2005), heart rate (Bunde et al., 2000), cloud dynamics (Ivanova et al., 2000), wind speed data (Govindan and Kantz, 2004), rainfall time series (Matsoukas et al., 2000) and magnetic field variations (Varotsos et al., 2009).

The DFA procedure comprises the following steps:

1) Seismoacoustic signal $x(i)$, where $i = 1, 2, 3,\ldots, N$ is assumed and converted to a random walk process by subtracting the mean value $\langle x \rangle$ and calculating the cumulative sum using:

$$y(i) = \sum_{k=1}^{i} \left[x(k) - \langle x \rangle \right] \tag{1}$$

2) The series $y(i)$ is converted to N_s nonoverlapping segments, each containing s points. Since the length of the series N may not be a multiple of s, a short part at the end of the series will remain in most cases. In order to consider such part, the same procedure is repeated starting from the other end of the series. Thus, $2 N_s$ segments are obtained altogether.

3) Define the local trend for each N_s segments v by a least-square fit of the data and calculate the detrended time series for segment duration s, denoted by $y_s(i)$, as the difference between the original time series and the fit,

$$y_s(i) = y(i) - p_v(i) \tag{2}$$

where $p_v(i)$ is the fitting polynomial in segment v.

4) Calculate for each $2 N_s$ segments the variance

$$F_s^2(v) = \frac{1}{s} \sum_{i=1}^{s} \left\{ y_s \left[(v-1)s + i \right] \right\}^2 \tag{3}$$

of the detrended series $y_s(i)$ by averaging over all data points i in v^{th} segment.

5) Average over all segments and take the square-root to calculate the DFA fluctuation function

$$F(s) = \left[\frac{1}{2N_s} \sum_{v=1}^{2N_s} F_s^2(v) \right]^{1/2} \tag{4}$$

If the time series is governed by long-range power-law correlation, the fluctuation functions $F(s)$ increase by a power-law

$$F(s) \propto s^H \tag{5}$$

The log-log plot of $F(s)$ versus s gives a straight line with slope H, known as the Hurst exponent (Hurst et al., 1965; Feder, 1988; Kantelhardt et al., 2002). We should mention that fluctuation exponent α_{DFA} in original papers (Peng et al., 1994; Kantelhardt et al., 2001) corresponds to Hurst exponent as $H = \alpha_{\text{DFA}}$ for fractional Gaussian noise and as $H = \alpha_{\text{DFA}} - 1$ for fractional Brownian motion (Seuront, 2010; Zhang et al., 2008). If only short-range correlations (or no correlations) exist in the series, then the fluctuation exponent H is equal to 0.5; $0.5 < H < 1$ indicates long memory or persistence and $0 < H < 0.5$ indicates short memory or anti-persistence (Peng et al., 1994; Zhang et al., 2008).

3.2. Multifractal detrended fluctuation analysis

Multifractal detrended fluctuation analysis (MDFA) is a generalization of standard DFA by identifying the scaling of the qth-order moments of the time series (Kantelhardt et al., 2002).

It is widely used when time series has not a simple monofractal scaling behavior, but exhibits more complicated one, when different parts of time series characterized by different scaling exponents: *e.g.* streamflow series (Zhang et al., 2008), seismic interevent times of earthquakes (Chamoli and Yadav, 2015), seismograms (Padhy, 2006), volcanic signals during pre- and eruptive phases (Telesca et al., 2015).

The first four steps (Eqs. (1)–(3)) in MDFA procedure are the same as those in the standard DFA. In the fifth step, we average over all segments to obtain the qth-order fluctuation function as:

$$F_q(s) = \left[\frac{1}{2N_s} \sum_{v=1}^{2N_s} \{F_s^2(v)\}^{q/2} \right]^{1/q} \tag{6}$$

where, in general, the index variable q may take any real number except zero. For $q = 0$, $F_q(s)$ cannot be determined by the normal averaging procedure of Eq. (6) because of the diverging exponent. Instead, a logarithmic averaging procedure is applied to get:

$$F_0(s) = exp \left(\frac{1}{4N_s} \sum_{v=1}^{2N_s} ln\left[F_s^2(v) \right] \right) \approx s^{H_{q=0}} \tag{7}$$

If the time series is long-range power-law correlated, $F_q(s)$ increases for large values of s as a power-law

$$F_q(s) \propto s^{H_q} \tag{8}$$

The log-log plot of $F_q(s)$ versus s gives a straight line with slope H_q, known as the generalized Hurst exponent, for a given value q (Kantelhardt et al., 2002; Telesca et al., 2015; Padhy, 2016). In general, H_q will depend on q. In particular, for monofractal series it is independent of q and for stationary time series, $H_q = 2$ is identical to Hurst exponent (Kantelhardt et al., 2002; Telesca et al., 2015) as Eq. (6) for $q = 2$ is equivalent to Eq. (4). For time series when small and large fluctuations scale differently (multifractality), H_q strongly depends on q. For positive values of q, the scaling behavior of segments with large fluctuations is characterized by a smaller scaling exponent H_q. On the contrary, for negative q values, the scaling exponent H_q describes the scaling behavior of segments with small fluctuations, usually characterized by larger scaling exponents (Kantelhardt et al., 2002).

The generalized Hurst exponent H_q is directly related to the classical or global scaling exponent t_q as:

$$t_q = qH_q - 1 \tag{9}$$

We can introduce the spectrum of local dimensions (Holder exponents or singularities) $f(\alpha)$, also called as multifractal spectrum, using Legendre transform:

$$f(\alpha) = q\alpha - t_q \tag{10}$$

where is the q-order singularity (Holder) exponent. The multifractal spectrum $f(\alpha)$ indicates the dimension of the subset of the series characterized by singularity strength α (Kantelhardt et al., 2002; Padhy, 2016) and its width expresses the range of the exponents, defined as $\Delta\alpha = \alpha_{max} - \alpha_{min}$, where α_{max} and α_{min} are the maximum and the minimum α-value. The more or less multifractality of the series (larger or smaller $\Delta\alpha$), the more or less heterogeneous the series (Telesca et al., 2015).

To illustrate the difference between typical monofractal noise and multifractal signal, we obtain their generalized Hurst exponent H_q functions and multifractal spectrum $f(\alpha)$ (Fig. 3).
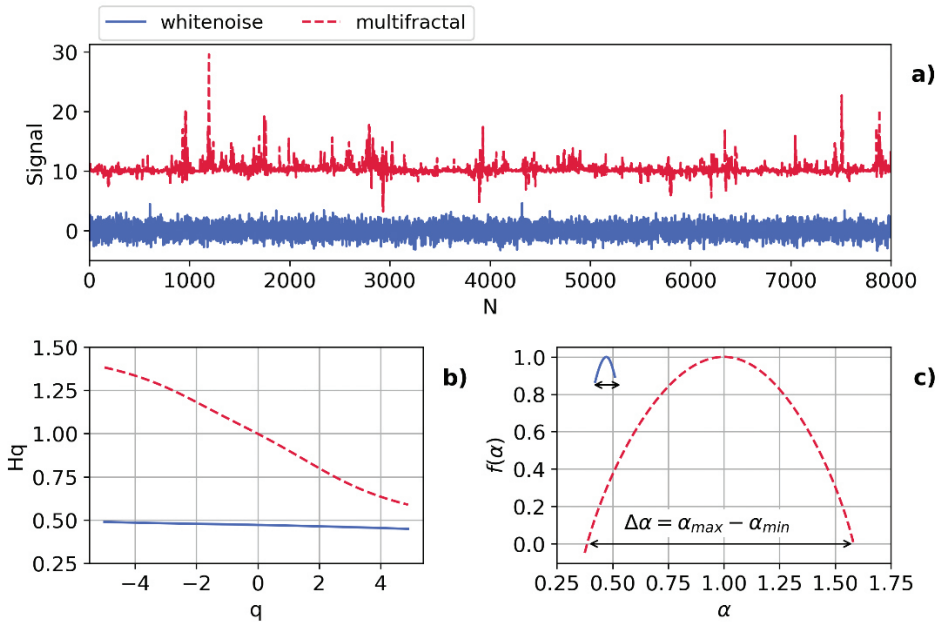
Figure 3. MDFA results for white noise and multifractal signal: (*a*) white noise and multifractal time series, (*b*) generalized Hurst exponent H_q functions, (*c*) multifractal spectrum (plot of generalized fractal dimension $f(\alpha)$ versus q-order singularity exponent α).

White noise characterized by almost constant value of H_q with very small variations around 0.5, which leads to linear q-dependency of t_q (Eq. 9), that further leads to almost constant α (tangent slope of t_q), which reduces multifractal spectrum to small arc with very small width ($\Delta\alpha_{whitenoise} = 0.1$). In contrast, the multifractal series has wide range of H_q with the wide multifractal spectrum in the form of large arc ($\Delta\alpha_{multifractal} = 1.21$). Also, these signals have different values of α_0 (the value of α corresponding to maximum $f(\alpha)$).

We used the q-order that weights the local variations in the acoustic signals, varying between –5 and 5. The value of polynomial order for detrending the time series was in range 1–3 and the minimum segment size was 16 for all DFA and MDFA procedures.

4. Results and discussion

We took one signal in each group: high, medium and low amplitude acoustic responses to the events SE1, SE3 and SE6 and analyzed their different parts, corresponding to seismic wave arrival and background noise (Fig. 4) on the basis of MDFA method (Fig. 5). Due to low signal-to-noise ratio, the moment of seismic wave arrival for the low amplitude signal (Fig. 4c) was highlighted approximately on the basis of the seismic event SE6 time from the catalogue.
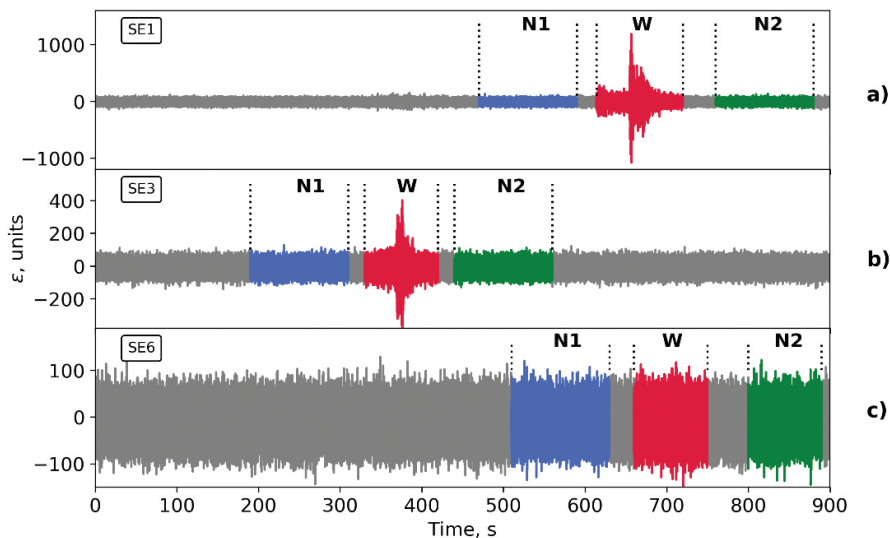
Figure 4. Acoustic signals and its parts corresponding to waveform and surrounding background noise: (*a*) high amplitude acoustic response to seismic event SE1 (record starting: 23.05.2018, 01:28:26 UTC); (*b*) medium amplitude signal for SE3 (record starting: 29.12.2017, 19:16:04 UTC); (*c*) low amplitude signal for SE6 (record starting: 13.12.2017 01:50:39 UTC). Waveform (W) - red line; background noise before (N1, blue line) and after (N2, green line) seismic wave arrival.
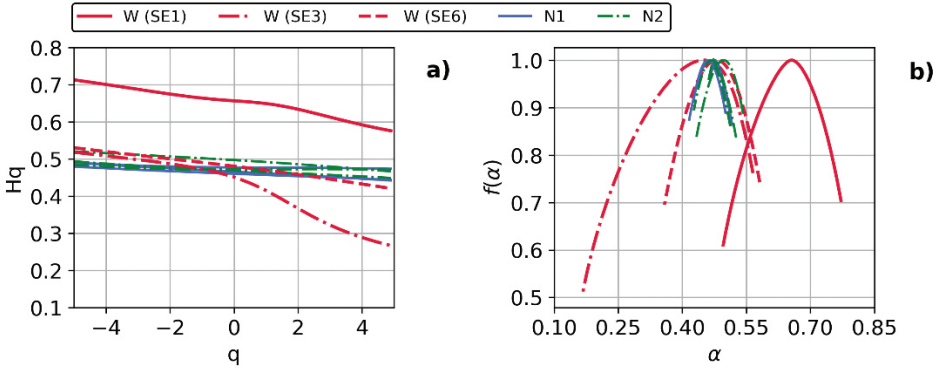
Figure 5. MDFA results for waveform (W) and background noise (N1, N2) parts of high (SE1), medium (SE3) and low amplitude (SE6) seismoacoustic signals: (*a*) generalized Hurst exponent H_q, (*b*) multifractal spectrum $f(\alpha)$.

As one would expect, background noise parts (N1, N2) have the values of generalized Hurst exponent H_q almost be constant with small variations around 0.5 (Fig. 5a) and very small width of the multifractal spectrum $\Delta\alpha_{N1}$, $N_2 \approx 0.1$ (Fig. 5b), being similar to white noise signal (see Figs. 3b–c).

In contrast, the values of multifractal spectrum width is larger for parts related to seismic wave arrival (W) than those for the background noise ($\Delta\alpha_{W(SE1)}$ = 0.28, $\Delta\alpha_{W(SE3)}$ = 0.40, $\Delta\alpha_{W(SE6)}$ = 0.22) and the values of H_q also have wider range, except for low amplitude signal W(SE6), probably, due to low signal-to-noise ratio. The long left tail of the multifractal spectrum of the waveforms indicates that these time series have a multifractal structure that is insensitive to the local fluctuations with small magnitudes and its dynamics is dominated by the large fluctuations (Padhy, 2016). This right truncation of the multifractal spectrum originates from the leveling of the H_q for negative q values (Fig. 5a).

Further, we analyzed three different parts of the high amplitude signal, corresponding to acoustic response to different phases of seismic wave: P-wave, S- and surface wave, coda wave (Fig. 6).

We found that the P-wave and S- and surface wave parts are characterized by wider range of values of generalized Hurst exponent H_q and wider multifractal spectrum ($\Delta\alpha_P$ = 0.37, $\Delta\alpha_S$ = 0.35) in comparison to coda part, which has almost constant H_q for all values of q, and minimal width of multifractal spectrum ($\Delta\alpha_{CODA}$ = 0.13). Such monofractal behavior of coda wave part is probably due to smaller changes in waveform amplitude against its background than those for P-, S- and surface waves. P- and S-parts have almost the same width of multifractal spectrum, but differ in range of H_q and values of α_0 (α_{0P} = 0.72, α_{0S} = 0.91), which can be used to differentiate these phases of seismic wave arrival.
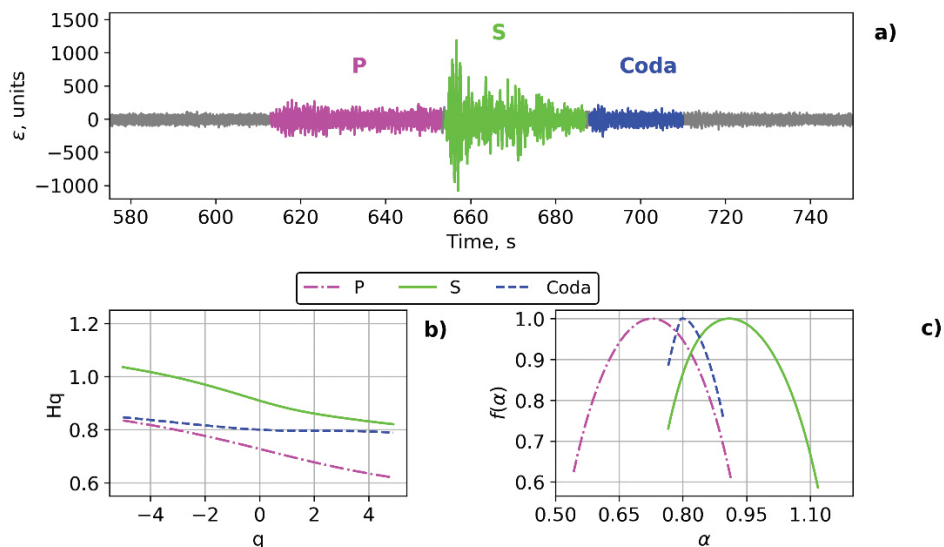
Figure 6. Acoustic response to different phases of seismic wave (*a*) and their multifractal characteristics (*b*) generalized Hurst exponent, H_q, (*c*) multifractal spectrum $f(\alpha)$.

We found that the multifractal parameters, such as $\Delta\alpha$ and α_0, could be used: (i) to detect the moment of seismic wave arrival, (ii) estimate its duration and (iii) separate different phases of waveform, such as P-, S- and coda waves, especially for low amplitude acoustic response signals, characterized by unclear waveform. To test this approach, we used MDFA in moving window (~ 2 sec) to obtain time series of $\Delta\alpha$ and α_0 (Fig. 7) for high amplitude signal (SE1). To highlight the main features we performed moving window smoothing (window size = 10). We chose this signal to compare the moments of signal amplitude burst with the moments of $\Delta\alpha$, α_0 values increase, as the different parts of waveform might have
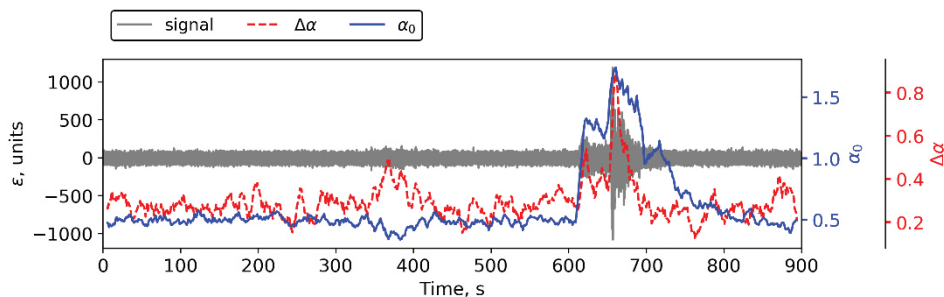
Figure 7. Temporal variations in $\Delta\alpha$ (dashed red line) and α_0 (solid blue line) calculated for high amplitude acoustic signal (SE1) (solid grey line).

the different multifractal spectrum, particularly, in comparison with the background noise, which has constant and much smaller values of $\Delta\alpha$, α_0.

Part of the signal, corresponding to background noise before and after the seismic wave arrival demonstrate monofractal behavior, characterized by almost constant α_0 values around 0.5 and small width of multifractal spectrum ~ 0.2 similar to white noise (Fig. 3b). The moment of seismic wave arrival is indicated in both time-series by sharp increase in $\Delta\alpha$ and α_0 values, relating to P-wave segment, which exhibits multifractal behavior. Further increase in $\Delta\alpha$ values describes increase of multifractality degree, corresponding to S-wave arrival. We should also note that the coda wave is not clearly distinguished from the background noise in temporal variations of $\Delta\alpha$, while the time series of α_0 shows three distinct segments: the first two for P- and S-waves and the last one, corresponding to coda part with much slower decay up to the background values.

As the Hurst exponent defined by the monofractal DFA expresses the average fractal structure of the signal and is closely related to the central tendency of multifractal spectrum, we can use DFA procedure in small moving windows and detect the moments of change in multifractal spectrum central tendency. We obtained results, similar to variations of α_0 (Fig. 7) by using monofractal DFA, characterizing transition from monofractal behavior with independent of short-range dependent structure with Hurst exponent $H = 0.5$ into the long-range dependent (*i.e.*, correlated) structure with non-stationary behavior (Fig. 8).

We used this procedure for the rest of the signals (SE2-SE6) to obtain variations of Hurst exponent before, during and after the seismic wave arrival (Fig. 9).

We can observe small fluctuations of Hurst exponent around white noise level ($H = 0.5$), then stepwise increase, coinciding with arrival of different phases of the seismic wave (SE2, SE3 and SE4) with subsequent decay to the background level. It is particularly useful in analysis of acoustic response to the seismic event, when the moment of seismic wave arrival is not evident due to
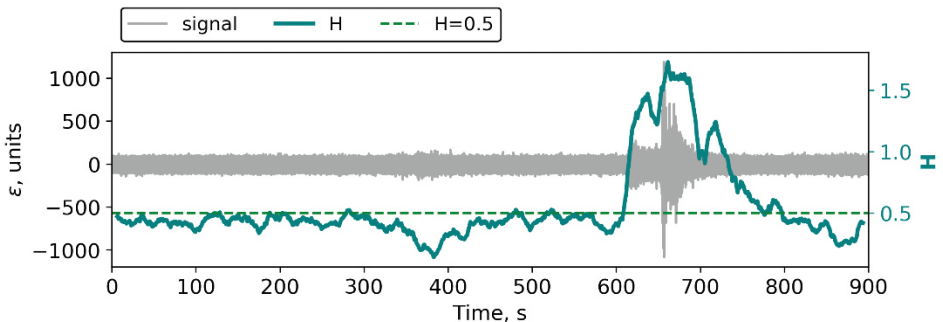
Figure 8. Temporal variations in Hurst exponent (solid green line) for high amplitude acoustic signal (SE1) (solid grey line). The dashed line: $H = 0.5$ level.

the low signal-no-noise ratio, *e.g.* signals for SE5 and SE6. The stepwise change of H values for these low amplitude signals, probably can be an evidence of P- and S-wave arrival, which are the measure of heterogeneities of the medium of different scales (*i.e.* multifractality) (Padhy, 2016).

In order to investigate the origin of multifractality of these low amplitude signals, we calculated 5 random surrogates of the signal for SE6 (Fig. 10). Surrogates were obtained from the original time series by random shuffling its values.

Each of the surrogates has the same probability density function, but not the correlation properties, as they are destroyed during the random shuffling. If multifractal properties depend on the long-range correlations, the shuffled series exhibits monofractal behavior (Padhy, 2016; Telesca et al., 2015). We can observe that the surrogates have the multifractal spectra different from the original signal with smaller width ($\Delta\alpha_{W(SE6)} = 0.22 > \Delta\alpha_{W(SE6)\,shuffled} \approx 0.1$) and narrower
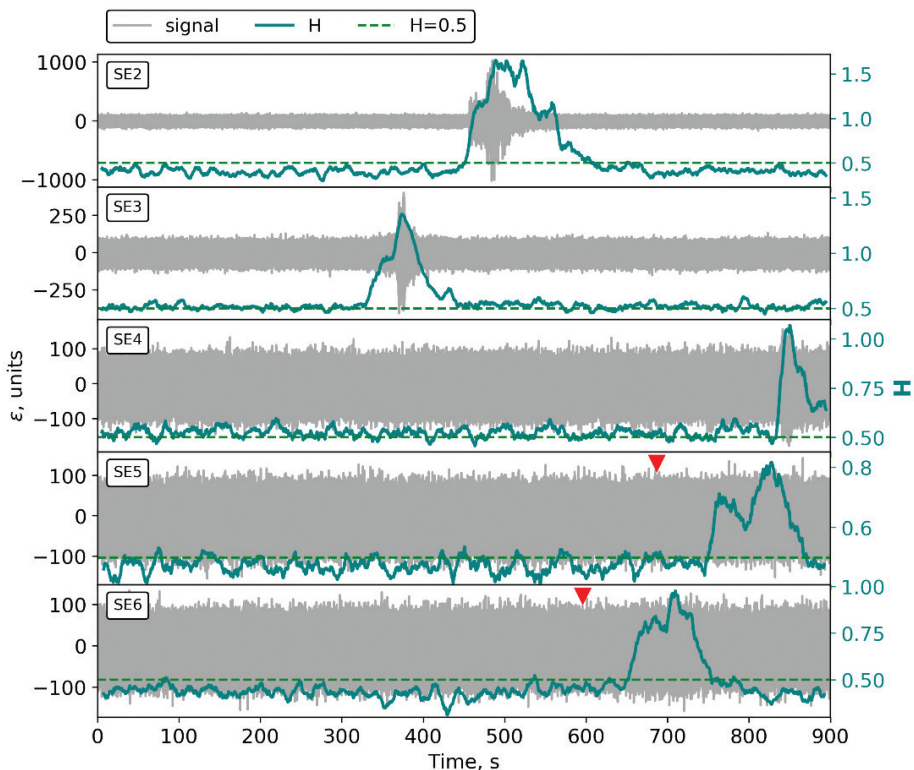
Figure 9. Temporal variations in Hurst exponent (solid green line) for high (SE2), medium (SE3, SE4) and low (SE5, SE6) amplitude acoustic signals (solid grey line). The dashed line: $H = 0.5$ level. Red triangle indicates the time of seismic event according to the seismic catalogue.
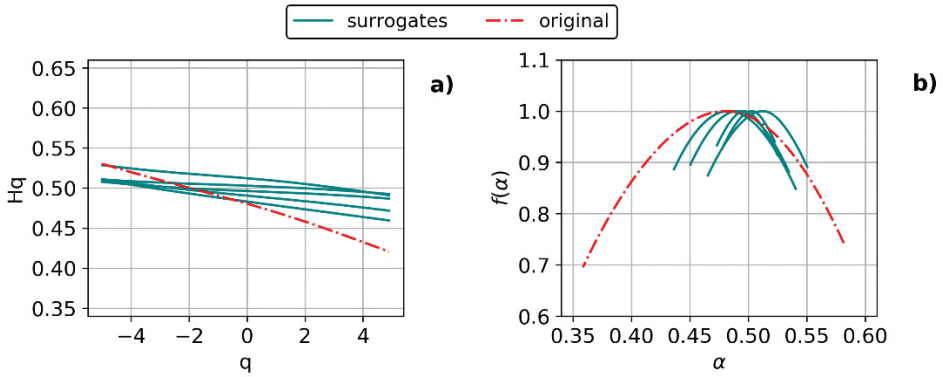
Figure 10. Comparison of the generalized Hurst exponents (*a*) and the multifractal spectra (*b*) of original acoustic response to SE6 and its five randomly shuffled surrogates.

range of generalized Hurst exponent values, expressing mainly monofractal behavior. These results confirm that the multifractal properties of the seismoacoustic signal are not obtained by chance and dominantly due to long-range correlations of fluctuations, which was used to detect the moments of seismic wave arrival and distinguish its different phases, such as P-, S- and coda waves.

5. Conclusions

The fractal properties of seismoacoustic signals of various amplitudes were analyzed by using mono- and multifractal detrended fluctuation analysis. Both methods showed that the acoustic response to the seismic wave passing through the measuring station differs from the surrounding background noise in scaling exponent values and multifractal spectrum width. The background noise before and after the seismic wave arrival was characterized by narrow width of the multifractal spectrum ($\Delta\alpha \approx 0.1$) and almost constant generalized Hurst exponent ($H_q \approx 0.5$), exhibiting monofractal behavior similar to white noise. Multifractal properties are more pronounced for high amplitude signals with clear P-, S- and coda waves, although the low amplitude signals with unclear waveform have sufficiently different multifractal spectrum and Hurst exponent values to differentiate them from background noise. Comparison of the multifractal spectrum of the low amplitude signal segment, containing seismic wave arrival with its randomly shuffled surrogates showed that the origin of multifractality in the segment is predominantly due to long-range correlation of fluctuations within it. Our analysis showed that the fractal properties of seismoacoustic signals can be applied in detection of the moment of seismic wave arrival; estimation of the waveform duration; and in distinguishing its different phases, such as P-, S- and coda waves, especially in case of low amplitude acoustic signals.

References

Adushkin, V. V. and Spivak, A. A. (2012): Near-surface geophysics: Complex investigations of the lithosphere-atmosphere interactions, *Izv. – Phys. Solid Earth*, **48**, 181–198, DOI: 10.1134/S1069351312020012.

Buldyrev, S. V., Goldberger, A. L., Havlin, S., Mantegna, R. N., Matsa, M. E., Peng, C. K., Simons, M. and Stanley, H. E. (1995): Long-range correlation properties of coding and noncoding DNA sequences: GenBank analysis, *Phys. Rev. E*, **51**, 5084–5091, DOI: 10.1103/PhysRevE.51.5084.

Bunde, A., Havlin, S., Kantelhardt, J. W., Penzel, T., Peter, J. H. and Voigt, K. (2000): Correlated and uncorrelated regions in heart-rate fluctuations during sleep, *Phys. Rev. Lett.*, **85**, 3736–3739, DOI:10.1103/PhysRevLett.85.3736.

Carpinteri, A., Lacidogna, G. and Niccolini, G. (2009): Fractal analysis of damage detected in concrete structural elements under loading, *Chaos Soliton Fract.*, **42**, 2047–2056, DOI: 10.1016/j.chaos.2009.03.165.

Chamoli, A. and Yadav, R. B. S. (2015): Multifractality in seismic sequences of NW Himalaya, Nat. Hazards, **77**, 19–32, DOI: 10.1007/s11069-013-0848-y.

Dolgikh, G. I., Kuptsov, A. V., Larionov, I. A., Marapulets, Y. V., Shvets, V. A., Shevtsov, B. M., Shirokov, O. P., Chupin, V. A. and Yakovenko, S. V. (2007): Deformation and acoustic precursors of earthquakes. *Dokl. Earth Sc.*, **413**, 281–285, DOI: 10.1134/S1028334X07020341.

Feder, J. (1988): *Fractals*. Springer US, Boston, MA, 284 pp, DOI: 10.1007/978-1-4899-2124-6.

Gadre, V. M., Dimri, V. M. and Chandrasekhar, E. (2014): *Wavelets and fractals in earth system sciences.* Taylor & Francis, Boca Raton, FL, 286 pp.

Govindan, R. B. and Kantz, H. (2004): Long-term correlations and multifractality in surface wind speed. *Europhys. Lett.*, **68**, 184–190, DOI: 10.1209/epl/i2004-10188-3.

Gregori, G. P., Poscolieri, M., Paparo, G., Simone, S., Rafanelli, C. and Ventrice, G. (2010): "Storms of crustal stress" and AE earthquake precursors, *Nat. Hazards Earth Syst. Sci.*, **10**, 319–337, DOI: 10.5194/nhess-10-319-2010.

Hurst, H. E., Black, R. P. and Simaika, Y. M. (1965): *Long-term storage: An experimental study.* Constable, London, 145 pp.

Ivanova, K., Ausloos, M., Clothiaux, E. E. and Ackerman, T. P. (2000): Break-up of stratus cloud structure predicted from non-Brownian motion liquid water and brightness temperature fluctuations, *Europhys. Lett.*, **52**, 40–46, DOI: 10.1209/epl/i2000-00401-5.

Kantelhardt, J. W., Koscielny-Bunde, E., Rego, H. H. A., Havlin, S. and Bunde, A. (2001): Detecting long-range correlations with detrended fluctuation analysis, *Physica A*, **295**, 441–454, DOI: 10.1016/S0378-4371(01)00144-3.

Kantelhardt, J. W., Zschiegner, S. A., Koscielny-Bunde, E., Havlin, S., Bunde, A. and Stanley, H. E. (2002): Multifractal detrended fluctuation analysis of nonstationary time series, *Physica A*, **316**, 87–114, DOI: 10.1016/S0378-4371(02)01383-3.

Király, A. and Jánosi, I. M. (2005): Detrended fluctuation analysis of daily temperature records: Geographic dependence over Australia, *Meteorol. Atmos. Phys.*, **88**, 119–128, DOI: 10.1007/s00703-004-0078-7.

Kuptsov, A. V. (2005): Variations in the geoacoustic emission pattern related to earthquakes on Kamchatka, *Izv. – Phys. Solid Earth*, **41**, 825–831.

Larionov, I. A., Marapulets, Y. V. and Shevtsov, B. M. (2014): Features of the Earth surface deformations in the Kamchatka peninsula and their relation to geoacoustic emission, *Solid Earth*, **5**, 1293–1300, DOI: 10.5194/se-5-1293-2014.

Lu, C., Mai, Y.-W. and Xie, H. (2005): A sudden drop of fractal dimension: A likely precursor of catastrophic failure in disordered media, *Philosophical Magazine Letters*, **85**, 33–40, DOI: 10.1080/09500830500153883.

Marapulets, Y. V., Rulenko, O. P., Larionov, I. A. and Mishchenko, M. A. (2011): Simultaneous response of high-frequency geoacoustic emission and atmospheric electric field to strain of near-surface sedimentary rocks, *Dokl. Earth Sc.*, **440**, 1349–1352, DOI: 10.1134/S1028334X11090285.

Matsoukas, C., Islam, S. and Rodriguez-Iturbe, I. (2000): Detrended fluctuation analysis of rainfall and streamflow time series, *J. Geophys. Res.*, **105**, 29165–29172, DOI: 10.1029/2000JD900419.

Padhy, S. (2016): The multi-fractal scaling behavior of seismograms based on the detrended fluctuation analysis, in *Fractal solutions for understanding complex systems in Earth sciences*, edited by Dimri, V. P. Springer Earth System Sciences. Springer, Cham, 99–115, DOI: 10.1007/978-3-319-24675-8_7.

Paparo, G., Gregori, G.P., Poscolieri, M., Marson, I., Angelucci, F. and Glorioso, G. (2006): Crustal stress crises and seismic activity in the Italian peninsula investigated by fractal analysis of acoustic emission, soil exhalation and seismic data, *Geol. Soc. London Spec. Publ.*, **261**, 47–61, DOI: 10.1144/GSL.SP.2006.261.01.04.

Peng, C.-K., Buldyrev, S. V., Havlin, S., Simons, M., Stanley, H. E. and Goldberger, A. L. (1994): Mosaic organization of DNA nucleotides, *Phys. Rev. E*, **49**, 1685–1689, DOI: 10.1103/PhysRevE.49.1685.

Rulenko, O. P., Marapulets, Y. V. and Mishchenko, M. A. (2014): An analysis of the relationships between high-frequency geoacoustic emissions and the electrical field in the atmosphere near the ground surface, *J. Volcanolog. Seismol.*, **8**, 183–193, DOI: 10.1134/S0742046314030051.

Seuront, L. (2010): *Fractals and multifractals in ecology and aquatic science*. Taylor & Francis, Boca Raton, 360 pp.

Talkner, P. and Weber, R. (2000): Power spectrum and detrended fluctuation analysis: Application to daily temperatures, *Phys. Rev. E*, **62**, 150–160, DOI: 10.1103/PhysRevE.62.150.

Telesca, L., Lovallo, M., Martì Molist, J., López Moreno, C. and Abella Meléndez, R. (2015): Multi-fractal investigation of continuous seismic signal recorded at El Hierro volcano (Canary Islands) during the 2011–2012 pre- and eruptive phases, *Tectonophysics*, **642**, 71–77, DOI: 10.1016/j.tecto.2014.12.019.

Turcotte, D. L. (1997): *Fractals and chaos in geology and geophysics*. 2nd edition, Cambridge University Press, Cambridge, U. K., New York, 398 pp.

Varotsos, P. A., Sarlis, N. V. and Skordas, E. S. (2009): Detrended fluctuation analysis of the magnetic and electric field variations that precede rupture. *Chaos: An Interdisciplinary Journal of Nonlinear Science*, **19**, 23114, DOI: 10.1063/1.3130931.

Zakupin, A. S., Bogomolov, L. M., Mubassarova, V. A. and Il'ichev, P. V. (2014): Seismoacoustic responses to high-power electric pulses from well logging data at the Bishkek geodynamical test area, *Izv. - Phys. Solid Earth*, **50**, 692–706, DOI: 10.1134/S1069351314040193.

Zhang, Q., Xu, C.-Y., Chen, Y. D. and Yu, Z. (2008): Multifractal detrended fluctuation analysis of streamflow series of the Yangtze River basin, China, *Hydrol. Process.*, **22**, 4997–5003, DOI: 10.1002/hyp.7119.

URL1: Piezoelectric geophones A16XX and A05XX, last available on 27 May 2019 at http://geophone.narod.ru/PDF/Geophones_AXXXX.pdf

SAŽETAK

Fraktalna analiza seizmoakustičnih signala u sedimentnim stijenama blizu površine na Kamčatki

Sanjar Imashev, Mikhail Mishchenko i Mikhail Cheshev

U ovom smo radu mono- i multifraktalnom detrendiranom fluktuacijskom analizom (DFA) proučavali vremenske fluktuacije u dinamici seizmoakustičnih podataka zabilježenih na postaji Karymshina, koja je smještena u seizmički aktivnom području Kamčatke. U analizi smo koristili niz seizmoakustičnih odziva prilagođenih na regionalne potrese s magnitudama $M > 4$ za razdoblje 2017.–2018. Niz smo podijelili u tri grupe (visoka, srednja i niska) na temelju amplitude zabilježenog seizmoakustičnog odziva. Dio mikroseizmičkog nemira prisutnog unutar signala iskazuje monofraktalnu strukturu sličnu bijelom šumu s gotovo konstantnim vrijednostima generaliziranog Hurstovog eksponenta $H_q \approx 0{,}5$ i vrlo malom širinom multifraktalnog spektra $\Delta\alpha \approx 0{,}1$. Analiza seizmoakustičnog signala visoke amplitude s jasnim P-, S- i koda valovima pokazala je da P- i S-valovi pokazuju širi multifraktalni spektar ($\Delta\alpha P = 0{,}37$, $\Delta\alpha_S = 0{,}35$) i raspon generaliziranih Hurstovih eksponenata Hq u usporedbi s koda valovima, koje karakterizira gotovo konstantan Hq i minimalna širina multifraktalnog spektra ($\Delta\alpha_{\mathrm{CODA}} = 0{,}13$). Pokazali smo da se svojstva multifraktalnog spektra mogu upotrijebiti za otkrivanje nailaska seizmičkih valova, procjenu nihovog trajanja i razdvajanje P-, S- i koda valova. Primjena monofraktalne DFA metode na zapise u kliznom prozoru pokazala je da akustički signal prelazi iz monofraktalnog i nekoreliranog mikroseizmičkog nemira (Hurstov eksponent jednak 0,5) u stanje dugog dometa tijekom dolaska seizmičkih valova, što je korisno u analizi signala, posebno u slučaju akustičnih odziva niske amplitude s nejasnim valnim oblikom. Razlika u širini multifraktalnog spektra između izvornog signala niske amplitude i njegovih zamjenskih oblika, dobivenih nasumičnim odabirom, ukazuje da multifraktalnost u signalu dominantno ovisi o dalekosežnim korelacijama.

Ključne riječi: seizmoakustični signal, monofraktal, Hurstov eksponent, multifraktal, detrendirana fluktuacijska analiza

Corresponding author's address: Sanjar Imashev, Research Station of the Russian Academy of Sciences, Bishkek, 720049, Kyrgyzstan; ORCID: 0000-0003-3293-3764; tel: +996 312 613 140; e-mail: sanzhar.imashev@gmail.com.